Cross-shelf export of particulate organic carbon in the northern South China Sea: Insights from a ^{234}Th mass balance

Qingquan Hong [a,b,c], Shiyun Peng [a,b], Daochen Zhao [a,b], Pinghe Cai [a,b,*]

[a] State Key Laboratory of Marine Environmental Science, Xiamen University, Xiamen 361005, PR China
[b] College of Ocean and Earth Sciences, Xiamen University, Xiamen 361005, PR China
[c] School of Earth Sciences and Engineering, Nanjing University, Nanjing 210023, PR China

ARTICLE INFO

ABSTRACT

Cross-shelf transport of particulate organic carbon (POC) is an essential but poorly quantified process regulating the POC flux and the biological pump efficiency in marginal seas. Here, we estimated the cross-shelf export flux of ^{234}Th and POC from the northern South China Sea (NSCS) shelf based on a dataset of ^{234}Th in the water column and the underlying sediments over the shelf (bottom depth $\leq$ 200 m) and the adjacent slope (bottom depth > 200 m). Based on a full mass balance of ^{234}Th throughout the water column and the underlying sediments, we found that besides radioactive production and decay, sedimentary accumulation and cross-shelf export associated with drifting particles were the most important processes in the ^{234}Th budget. The input via horizontal shelf-slope water exchange and along-shelf water transport was a ^{234}Th source to the shelf water, and neglecting this component would underestimate the actual vertical ^{234}Th and POC fluxes by ~10–33%. The POC flux via vertical export from the euphotic zone was 26 $\pm$ 1 mmol m^{-2} d^{-1} while that via cross-shelf transport was 9.9 $\pm$ 3.4 mmol m^{-2} d^{-1}. The cross-shelf exported POC presumably inject into the intermediate/deep waters and could be trapped for several decades in the SCS. Our results highlight the importance of cross-shelf POC transport in regulating carbon storage in the SCS on seasonal to longer time scales. A compilation of the case studies regarding cross-shelf transport suggests its role in the carbon cycle might be more important than previously recognized and needs to be re-evaluated.

1. Introduction

Transport of particulate organic carbon (POC) from the euphotic zone to the deep ocean is one of the crucial processes that drive the biological carbon pump (BCP) and modulate the oceanic uptake of atmospheric CO_2 (Honjo et al., 2014). Continental shelves receive tremendous loadings of carbon and nutrients that stimulate high primary production. They contribute to higher primary production (~15–21%; Jahnke, 2010) and CO_2 uptake (~17%; Cai, 2011) relative to their fraction in the global ocean area (~8%). Some photosynthetically fixed carbon is effectively remineralized within the shelf water or is deposited and accumulated into the shelf sediments. However, the remainder can be transported off-shelf via strong intermediate and benthic particle plumes facilitated by intense sediment resuspension or turbidity and gravity currents (Bacon et al., 1994; Jahnke, 2010). The off-shelf exported carbon is presumably stored in the intermediate and deep waters, which have residence times of several decades (Liu and

Gan, 2017; Ma et al., 2017; Shih et al., 2019; and references therein). As such, cross-shelf transport of POC could be a powerful mechanism that controls the BCP efficiencies on continental shelves (Wong et al., 2000). Globally, this process, to a certain extent, determines the capacity of carbon storage in marginal seas over seasonal to decadal time scales (Baumann et al., 2013; Jahnke, 2010; Lepore et al., 2007; Shih et al., 2019).

Cross-shelf transport of POC used to be the core topic of some programs, such as the Shelf Edge Exchange Program (SEEP) and Kuroshio Edge Exchange Processes (KEEP) (Falkowski et al., 1988; Walsh et al., 1988; Wong et al., 2000). However, previous studies using the traditional sediment trap method could underestimate this cross-shelf flux and the BCP efficiencies in marginal seas. The short-lived particle reactive radionuclide ^{234}Th (half-life = 24.1 d) is a robust proxy of particle dynamics and export over the time scale of days to weeks (Waples et al., 2006). Unlike ^{234}Th, its long-lived parent uranium-238 is soluble and conservatively distributed with respect to salinity in the

---

ocean (Chen et al., 1986; Pates and Muir, 2007). As a result, effective scavenging and particle export create a [234]Th deficit relative to [238]U in the upper ocean. This deficit can be applied to estimate the vertical flux of POC with an appropriate model (Savoye et al., 2006) when the POC to [234]Th ratio in sinking particles at the export horizon of interest is measured (Buesseler et al., 2006). Similarly, a full mass balance of [234]Th in the water column and the underlying sediment package has excellent potential in quantifying the cross-shelf fluxes of particles and associated POC in shelf systems with the measured POC to [234]Th ratio in the particles at the shelf-slope boundary (Baumann et al., 2013; Lepore et al., 2007).

The northern South China Sea (NSCS) has broad continental shelves and an abyssal basin with water depths of up to ~4500 m. The monsoonal-driven surface gyres effectively reduce the supply of terrestrial nutrients to the basin. As a result, the basin is oligotrophic with low primary production while the shelf is more productive (Chen, 2005). Previous studies on POC mainly focus on the spatial/temporal variation of the downward flux from the euphotic zone and its controlling mechanisms (e.g., Cai et al., 2015b; Chen et al., 2008; Shih et al., 2019; Wei et al., 2011; Zhou et al., 2013, 2020). Lateral transport of POC into the deep NSCS is evidenced by elevated POC fluxes in the intermediate and deep waters (e.g., Ma et al., 2017; Shih et al., 2019; and references therein). The laterally-exported POC could be stored in the ocean for millennia via various processes, such as deposition and accumulation into the deep sediments or being utilized as a major energy and organic carbon source for the enhanced dark carbon fixation in the deep ecosystem (Shen et al., 2020). Nevertheless, the magnitude of the cross-shelf POC flux and its influence on the BCP efficiencies remains to be quantified. Here, we measured the [234]Th activities in the water column and the underlying sediments over the NSCS shelf. We constructed a full mass balance of [234]Th to estimate the cross-shelf flux of POC and evaluate its role in regulating the BCP efficiency in the NSCS.

2. Materials and methods

2.1. Sample collection

Water column and sediment core samples were collected over three cross-shelf transects in the NSCS during the summer of 2012 (Fig. 1).

Water samples for total and particulate [234]Th were collected throughout the water column. Sediment sampling using a box corer ($50 \times 50 \times 80$ cm^3) was attempted over the shelf. Unfortunately, we failed to retrieve sediment samples at some stations where the sediments are characterized by coarse gravel (Zhong et al., 2017). Sediment samples were checked visually to assure that the sediment–water interface was intact. Sediment sub-cores were retrieved by inserting transparent acrylic tubes (inner diameter = 65 mm, length = 30 cm) into the bulk sediments. Sub-cores were sectioned with intervals of 0.5 cm in the upper 1 cm and 1 cm below. Sediment sub-samples were freeze-dried, grounded, and homogenized before the analysis of excess [234]Th ([234]Th$_{ex}$).

2.2. [234]Th analyses

The procedure for determining total and particulate [234]Th was detailed in our prior studies (Cai et al., 2006b, 2010). Total [234]Th activities in seawater (4 L) were analyzed using the small-volume MnO$_2$ coprecipitation method with a [230]Th spike (Cai et al., 2006b; Pike et al., 2005). For particulate [234]Th, ~4–8 L of seawater was filtered onto a precombusted QMA filter (diameter: 25 mm; pore size: 1.0 μm). All the [234]Th samples were dried, mounted under one layer of Mylar film and aluminum foil (density: ~7.2 mg cm^{-2}). Samples were counted onboard with gas flow proportional low-background beta counters (RISØ) for the initial [234]Th activities and at the same counters after 150 days for the final counts. After counting, the recovery of [230]Th was determined by inductively coupled plasma mass spectrometry (Agilent 7700x) after the addition of a [229]Th internal standard and chemical purification. The recoveries were high and stable ($94.1 \pm 4.2\%$, 1 SD, n = 112). All [234]Th data were decay and recovery-corrected and reported with uncertainties propagated from the counting as well as the errors associated with the detector efficiency and the chemical recovery (Eq. (S.5)). Thorium-234 activities were calibrated with seawater collected between 500 and 3000 m of the South East Asian Time-series Study (SEATS) station, which showed a secular equilibrium between [234]Th and [238]U (average [234]Th/[238]U ratio: 1.01 ± 0.05, 1 SD, n = 9). [234]Th data from our lab are in good agreement with the GEOTRACES inter-calibration results of [234]Th (Maiti et al., 2012). Uranium-238 activities were estimated using the relationship of [238]U (dpm L^{-1}) = (0.0713 ± 0.0012) × salinity (Pates and Muir, 2007). The associated uncertainties of ~3% for [238]U activities
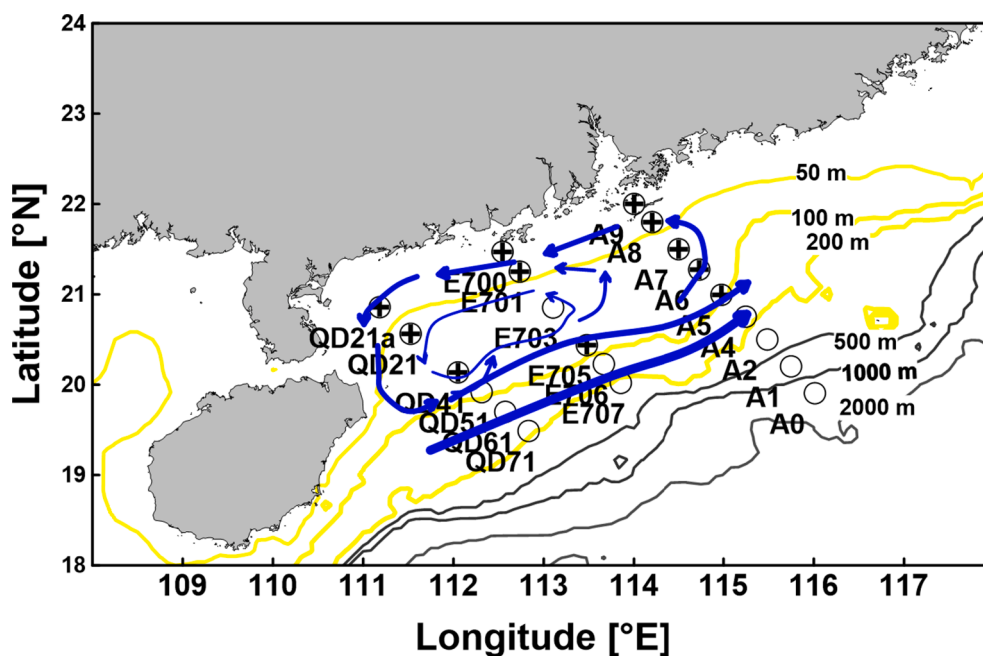

Fig. 1. Sampling locations of water column (open circle) and sediment (cross) in the northern South China Sea during the summer of 2012. The model-simulated surface currents (blue arrow) in summer were redrawn from Ding et al. (2017).

were propagated to the total ^{234}Th activities and the ^{234}Th/^{238}U ratios.

^{234}Th$_{ex}$ in sediments defined as the ^{234}Th unsupported by ^{238}U was determined involving two parallel measurements of duplicate samples: one upon return to the land-based laboratory (total ^{234}Th) and the other 5–6 months after the cruise (^{238}U-supported ^{234}Th). The procedure was detailed in our previous studies (e.g., Cai et al., 2014; Hong et al., 2017). Briefly, sediment samples (~5 g) were leached with 6 N HCl + H$_2$O$_2$ solution three times. After purification on an anion-exchange column (AG1-X8, 100–200 mesh), ^{234}Th was co-precipitated with MnO$_2$ and counted on beta counters. ^{234}Th$_{ex}$ was calculated as the difference between the two measurements. The chemical yield was assessed with a standard addition method that involves the measurement of replicate samples with a succession of ^{238}U–^{234}Th standard solutions (Cai et al., 2014). The regression of the measured ^{234}Th vs. ^{234}Th addition derived a high yield and low uncertainty (97.4 ± 7.0%), which was consistent with our previous determination (96.3 ± 5.9%; Cai et al., 2014) and indicated that the protocol is reliable for the measurement of ^{234}Th$_{ex}$. The reported ^{234}Th$_{ex}$ activities were decay-corrected to the sampling time, with associated errors propagated from the counting statistics, the counter efficiency, and the chemical yield.

2.3. POC analyses

After ^{234}Th analyses, the particulate samples were analyzed for POC according to the JGOFS protocols (Knap et al., 1996). The samples were acid-fumed with concentrated HCl to remove the carbonate fraction, and POC were determined with a PE-2400 SERIES II CHNS/O analyzer. The average blank was 5–8 μg C, which accounted for less than 5% of the POC measured in the samples. All the reported data were corrected for the blank. The precision for POC was better than 10% based on duplicate analyses of random samples.

2.4. Sediment porosity

Sediment porosity (ρ_S) was determined from the mass difference

before and after drying at 60 °C using a dry density of marine sedimsents (2.65 g cm^{-3}; Burdige, 2006).

2.5. Vertical flux of ^{234}Th and POC from the euphotic zone

2.5.1. Vertical flux of ^{234}Th

The change of ^{234}Th activity in the water column ($\frac{\partial A_{234Th_T}}{\partial t}$) can be described as a balance between the production from ^{238}U ($\lambda_{Th}A_U$) and the loss via decay ($\lambda_{Th}A_{234Th_T}$), particle export (P_{234Th}: dpm m^{-3} d^{-1}), and transport by advection and diffusion (V_{234Th}: dpm m^{-3} d^{-1}) as follows (Savoye et al., 2006):

$$\frac{\partial A_{234Th_T}}{\partial t} = \lambda_{Th} \times \left(A_U - A_{234Th_T} \right) - P_{234Th} + V_{234Th} \tag{1}$$

where A_{234Th_T} is the activity of total ^{234}Th (dpm m^{-3}), A_U is the ^{238}U sactivity (dpm m^{-3}), and λ_{Th} is the decay constant of ^{234}Th (0.02876 d^{-1}). Assuming a steady-state condition (i.e., $\frac{\partial A_{234Th_T}}{\partial t} = 0$), the vertical flux of ^{234}Th from an export horizon of interest ($P_{234Th@z}$: dpm m^{-2} d^{-1}) can be estimated with the equation:

$$P_{234Th@z} = \int_0^z \left[\lambda_{Th} \left(A_U - A_{234Th_T} \right) + V_{234Th} \right] dz \tag{2}$$

The export horizons were set to be 15/25, 50, and 75/100 m for the stations with bottom depths of ≤60 m, >60–110 m, and >110 m, respectively. They were roughly consistent with the bottom of the euphotic zone defined using PAR data but slightly shallower than those determined using fluorescence data (Table 1 and Fig. S.1). They lay above the benthic nepheloid layer (BNL; Fig. S.2). As such, the influence of sediment resuspension on the estimate of vertical fluxes of ^{234}Th and POC was minimized. Besides, they were similar to those set by Cai et al. (2015b) and allowed comparison between different cruises/seasons (Cai et al., 2015b; Chen et al., 2008).

Table 1
Depth of the euphotic zone (Ez), the selected export horizon, POC/^{234}Th$_P$ ratios in suspended particles (size: >1.0 μm) at the selected export horizon, residence time of total ^{234}Th with respect to scavenging in the euphotic zone (τ_t), ^{234}Th and POC fluxes, as well as the net primary production (NPP) from/in the euphotic zone in the northern South China Sea during the summer of 2012.

Station	Bottom depth [m]	Ez[a] [m]	Export horizon[b] [m]	^{234}Th flux [dpm m^{-2} d^{-1}]	POC/^{234}Th$_P$ [μmol dpm^{-1}]	POC flux [mmol m^{-2} d^{-1}]	τ_t [d]	NPP[c] [mmol m^{-2} d^{-1}]	Export efficiency [%]
A9	35	27(21)	15	1160 ± 30	41.7 ± 5.1	48.3 ± 6.5	2.8 ± 0.4	186 ± 90	26 ± 13
A8	47	—	15	460 ± 40	17.6 ± 1.8	8.1 ± 1.3	58 ± 6	104 ± 19	8 ± 2
A7	72	60(58)	50	2130 ± 70	23.8 ± 2.9	50.7 ± 6.9	28 ± 1	48 ± 9	106 ± 23
A6	89	50	50	1590 ± 70	9.4 ± 0.7	14.8 ± 1.5	49 ± 2	36 ± 5	41 ± 7
A5	103	67	50	1700 ± 60	7.2 ± 0.5	12.3 ± 1.1	42 ± 2	27 ± 2	46 ± 5
A4	187	94	100	2300 ± 130	7.6 ± 0.4	17.5 ± 1.5	76 ± 5	25 ± 1	72 ± 6
A2	395	102(70–108)	100	2080 ± 100	8.9 ± 0.6	18.4 ± 1.5	84 ± 4	22 ± 1	83 ± 7
A1	737	116(76–115)	100	670 ± 110	5.4 ± 0.4	3.6 ± 0.7	194 ± 3	21 ± 0	18 ± 3
A0	1418	92	100	130 ± 120	7.9 ± 0.6	1.0 ± 0.9	—	20 ± 0	5 ± 5
E700	26	20	15	1070 ± 40	43.9 ± 5.1	46.6 ± 6.6	8.8 ± 1	170 ± 30	28 ± 6
E701	45	33(38)	25	1070 ± 50	34.1 ± 7.3	36.3 ± 8.4	29 ± 2	102 ± 30	36 ± 14
E703	73	55	50	2090 ± 70	16.3 ± 2.1	33.9 ± 4.7	29 ± 1	28 ± 4	121 ± 24
E705	87	68	50	1860 ± 70	17.6 ± 1.5	32.7 ± 3.3	36 ± 1	23 ± 0	142 ± 13
E706	115	82	75	1680 ± 90	8.2 ± 0.6	13.8 ± 1.4	81 ± 4	22 ± 1	62 ± 6
E707	172	102(52–84)	100	1500 ± 100	7.1 ± 0.4	10.7 ± 1.1	133 ± 9	21 ± 1	51 ± 5
QD21a	38	—	15	900 ± 30	35.8 ± 6.7	32.2 ± 6.4	14 ± 1	91 ± 15	35 ± 9
QD21	60	46	25	740 ± 40	30.5 ± 6.0	22.6 ± 4.9	57 ± 3	47 ± 2	48 ± 10
QD41	89	68	50	890 ± 70	6.3 ± 0.4	5.5 ± 0.7	114 ± 10	27 ± 2	20 ± 3
QD51	101	80	50	1200 ± 70	28.4 ± 4.3	34.1 ± 5.9	74 ± 5	22 ± 0	156 ± 26
QD61	146	105	75	650 ± 110	19.9 ± 1.9	12.8 ± 2.8	262 ± 44	21 ± 0	60 ± 12
QD71	193	103	100	1160 ± 100	3.7 ± 0.2	4.3 ± 0.5	184 ± 17	21 ± 1	21 ± 2

a: The euphotic depth was determined with the 'primary production zone' method using *in situ* fluorescence data (Owens et al., 2015) or the 0.1–1% of the incident PAR density (in brackets); for the stations where 0.1% PAR level cannot be reached, only one value was presented.
b: The selected export horizons were roughly consistent with the bottom of the euphotic zone. For station QD51 and QD61, 50 and 75 m were selected respectively as the export horizon due to the influence of sediment resuspension (evidenced by high turbidity).
c: An 80-day average from 96 days before the sampling date, derived with VGPM using MODIS data. The uncertainties derive from the standard deviation of the 8-day products.

2.5.2. Vertical flux of POC

The vertical flux of POC ($P_{POC@z}$; mmol m^{-2} d^{-1}) can be determined by multiplying the ^{234}Th fluxes ($P_{^{234}Th@z}$) by the POC/^{234}Th$_P$ ratio in sinking particles at the export horizon (Buesseler et al., 2006):

$$P_{POC@z} = P_{^{234}Th@z} \times \left[\frac{POC}{^{234}Th_P} \right]_{@z}$$

In this study, POC/^{234}Th$_P$ ratios in sinking particles collected by pumps or traps were unavailable. Thus, we used the ratios in suspended particles (size > 1.0 μm) to derive POC fluxes, which was also applied to a high-resolution seasonal study (Cai et al., 2015b). It has been suggested that POC/^{234}Th$_P$ ratios in small particles (size: 1–10 μm and 10–53 μm; 0.96–9.4 μmol dpm^{-1}) were consistent, within a factor of 1–2, with those measured in large particles (size > 53 μm; 1.1–7.2 μmol dpm^{-1}) in the NSCS (Cai et al., 2006a). Besides, small particles dominate the particle reservoir (>90%) and bulk fluxes of ^{234}Th and POC (up to 80%) in the NSCS (Cai et al., 2006a; Hung and Gong, 2010), which is consistent with the significant contribution of small particles in carbon export (Le Moigne et al., 2013b; Puigcorbé et al., 2015; and references therein). As such, the utilization of the POC/^{234}Th$_P$ ratios in particles > 1 μm will provide a first-order estimate of the vertical POC fluxes in the dynamic shelf zone.

2.6. Calculation of net primary production (NPP) and the terms in the mass balance model of ^{234}Th

NPP was estimated with the standard Vertically Generalized Production Model (VGPM; Behrenfeld and Falkowski, 1997) using MODIS R2018 data (http://www.science.oregonstate.edu/ocean.productivity/standard.product.php). The terms in the ^{234}Th mass balance (total area, water volume, inventories of ^{234}Th and ^{238}U, vertical POC flux, and NPP) were calculated using a multiple triangle box approach (Fig. S.3; Tan et al., 2018). The details of the calculation were provided in the Supplementary Material.

3. Results

3.1. ^{234}Th/^{238}U disequilibrium in the water column

3.1.1. Distributions of ^{234}Th, TSM, and POC

Total and particulate ^{234}Th activities (^{234}Th$_T$ and ^{234}Th$_P$), POC concentrations, and potential temperature and salinity in the NSCS during the summer of 2012 are compiled in Table S.1. These parameters and the ^{234}Th$_T$/^{238}U activity ratios, as well as total suspended matter (TSM, filtered using polycarbonate membrane filters with a pore size of 0.45 μm) are shown in Fig. 2 and Fig. 3. Swimmers and microphytoplanktons were identified in some particulate samples (5 m at E703 and E705, 25 m at QD51) by the naked eye. They do not significantly bias the total ^{234}Th flux. However, these samples were excluded from the discussion since swimmers have notably high POC/^{234}Th$_P$ ratios and can significantly bias the POC flux (Buesseler et al., 2007). TSM and POC concentrations fell in the range of 0.03–3.34 mg L^{-1} and 0.79–12.7 μmol L^{-1}, respectively, and both decreased offshore (Fig. 3). POC concentrations were generally high in the surface water, while TSM showed elevated contents in the bottom layers. Remarkably high POC concentrations were observed throughout the water column in the innermost stations (closest to the shore in each section). ^{234}Th$_T$ varied from 0.15 ± 0.04 to 2.97 ± 0.09 dpm L^{-1} for all samples (Table S.1). Deficits of ^{234}Th were evident in the upper 100 m (Fig. 2). Below the euphotic zone, ^{234}Th deficits increased towards the seafloor on the shelf. The most pronounced deficit was observed in the bottom layers, with ^{234}Th$_T$ activity dropping to as low as ~0.2 dpm L^{-1} in the innermost stations. Strong gradients of turbidity in the bottom layers (Fig. S.2a) indicated the presence of a BNL in the area. The high concentrations of particles, together with pronounced ^{234}Th deficits (low ^{234}Th/^{238}U ratios) and elevated ^{234}Th$_P$/^{234}Th$_D$ ratios within the BNL (Fig. 3 and Fig. S.2c) suggest enhanced scavenging and cross-shelf export of ^{234}Th via strong particle plumes. Similar patterns in the shelf stations were observed in other cruises (Cai et al., 2015b; Chen et al., 2008). ^{234}Th excess (^{234}Th > ^{238}U) was measurable below ~100 m in the slope (Fig. 2), where contents of TSM and POC were low (Fig. 3). The excess may be related to the remineralization of the particles settling from the
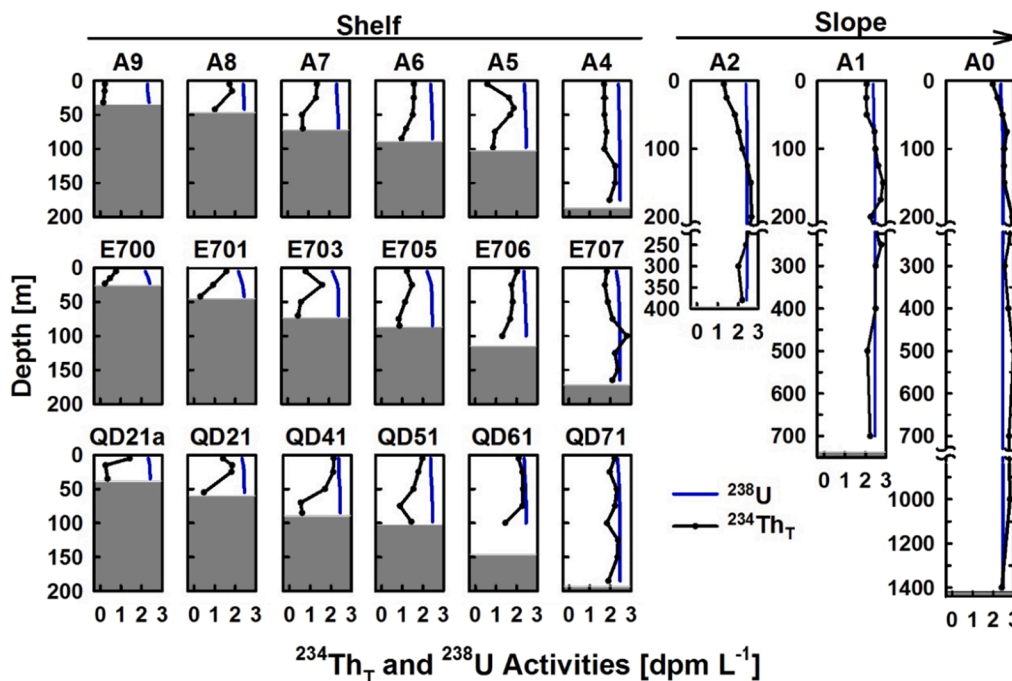

Fig. 2. Depth profiles of total ^{234}Th (^{234}Th$_T$) and ^{238}U in the water column of the northern South China Sea during the summer of 2012. The gray area denotes the bottom sediment. Error bars are shown if larger than the symbol size, but they are negligible on this scale.
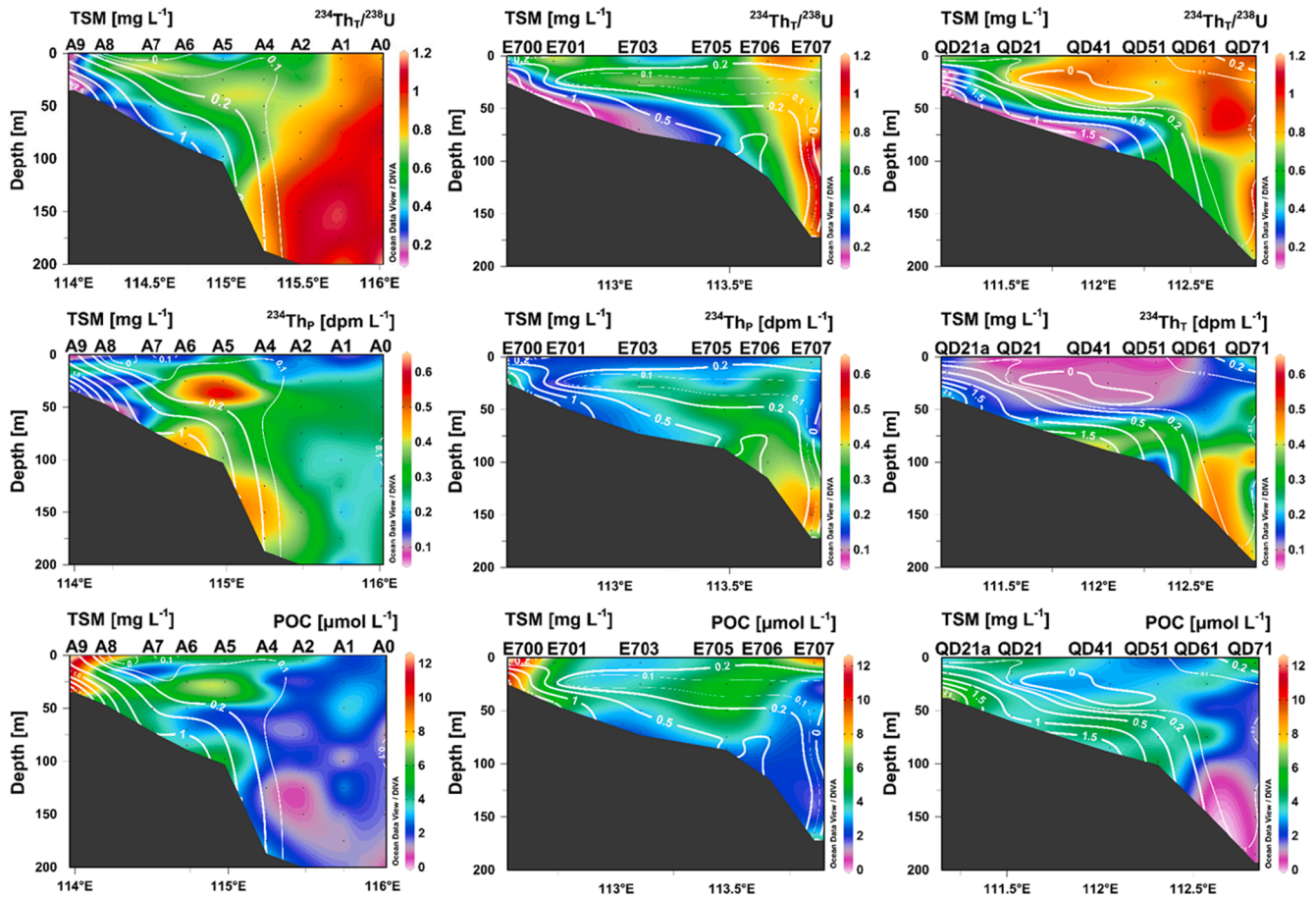
Fig. 3. Vertical distributions of $^{234}Th_T/^{238}U$ activity ratio, particulate ^{234}Th activity ($^{234}Th_P$), and POC concentration with TSM content (white contour line) in the northern South China Sea during the summer of 2012. Plots are created with Ocean Data View (Schlitzer, 2018).

euphotic zone or those laterally exported from the shelf.

3.1.2. ^{234}Th deficit and inventory in the water column

The site-specific deficit of ^{234}Th (Def $_{234Th}$: dpm m^{-2}) can be determined as the integral disequilibrium between ^{234}Th and ^{238}U in the water column:

$$\text{Def }_{234Th} = \int_0^z \left(A_U - A_{234Th_T}\right) dz \qquad (3)$$

^{234}Th deficits were integrated throughout the water column at the shelf stations and to the depth where ^{234}Th reached secular equilibrium with ^{238}U (~50–125 m) at the slope stations. ^{234}Th deficits (Fig. 4a; Table S.2) varied in the range of 4.3 ± 0.3–$12.1 \pm 0.3 \times 10^4$ dpm m^{-2} (average ± 1 SD: $7.9 \pm 2.3 \times 10^4$ dpm m^{-2}; n = 18) for the shelf stations and 0.9 ± 0.3–$7.0 \pm 0.4 \times 10^4$ dpm m^{-2} (average ± 1 SD: $3.3 \pm 3.2 \times 10^4$ dpm m^{-2}; n = 3) for the slope stations.

The site-specific ^{234}Th inventories ($I_i = \int_0^H A_{234Th_T} dz$) varied in 0.7–41.3×10^4 dpm m^{-2} (average ± 1 SD: $14.6 \pm 12.7 \times 10^4$ dpm m^{-2}; n = 18) for the shelf and 86.7–382×10^4 dpm m^{-2} (average ± 1 SD: $214 \pm 152 \times 10^4$ dpm m^{-2}; n = 3) for the slope (Table S.2). ^{234}Th inventories increased offshore due to the increase of $^{234}Th_T$ activities and bottom depth.

3.2. $^{234}Th_{ex}$ and the inventory in the sediment

$^{234}Th_{ex}$ was confined to the upper 5 cm of the sediment cores (Fig. 5). $^{234}Th_{ex}$ showed a rapid decrease downward the cores, which could be ascribed to the decay of ^{234}Th after deposition into the seabed. $^{234}Th_{ex}$ activities in the surficial 0–0.5 cm varied from 0.45 ± 0.11 to $7.20 \pm$

0.51 dpm g^{-1} and showed considerable spatial variability over the shelf. However, the distribution did not show a regular pattern with increasing distance offshore or bottom depth. These $^{234}Th_{ex}$ activities were comparable to those measured in the China coastal seas (Cai et al., 2015a, 2014; DeMaster et al., 1985; Hong et al., 2017; Huang et al., 2013; Wang et al., 2016).

The site-specific sedimentary inventories of $^{234}Th_{ex}$ presented remarkable spatial differences (Fig. 4b). However, no clear correlation was observed between inventories and the contents of silt and clay (Fig. S.4). The inventories (Table S.2) varied from 0.2 ± 0.1 to $9.4 \pm 1.0 \times 10^4$ dpm m^{-2} (average ± 1 SD: $3.6 \pm 3.1 \times 10^4$ dpm m^{-2}; n = 11). They fell within the range in China coastal seas (Cai et al., 2015a, 2014; Hong et al., 2017; Wang et al., 2016) and other marginal seas, such as the Long Island Sound, the Bering Sea, and the northwestern Iberian margin (Aller and Cochran, 2019; Baumann et al., 2013; Schmidt et al., 2002).

4. Discussion

4.1. ^{234}Th mass balance over the shelf of the NSCS

A full mass balance of ^{234}Th over the NSCS shelf was used to constrain particle transport rates during the summer of 2012 (Fig. 6). The processes responsible for the mass balance include continuous ^{234}Th production via radioactive decay of ^{238}U ($F_{Production}$), transport via water exchange, radioactive decay (F_{Decay}), particle accumulation into the underlying sediments (F_{Sed}), and cross-shelf export presumably associated with drifting particles within the BNL ($F_{Lateral}$). The mass balance model neglects the input of ^{234}Th from riverine freshwater discharge
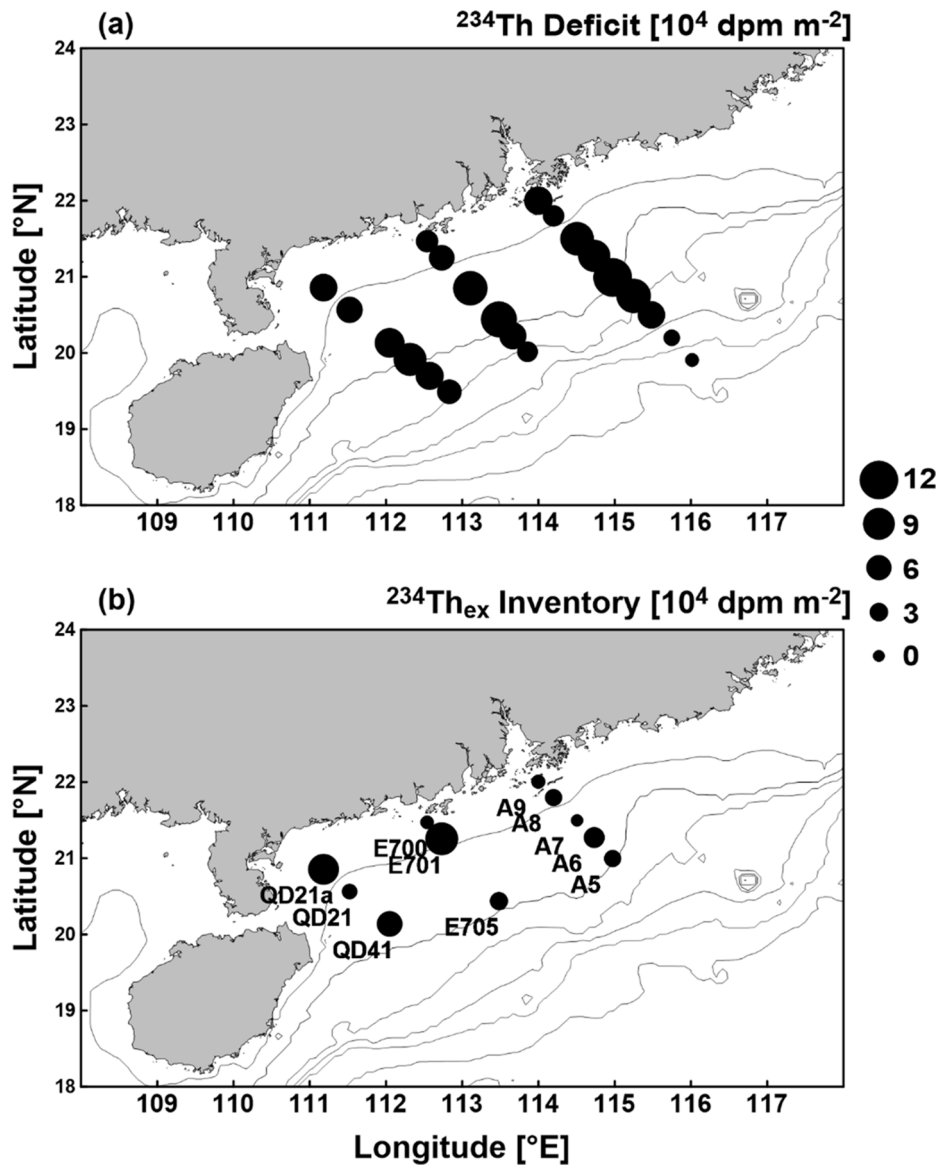
Fig. 4. Site-specific ^{234}Th deficit in the water column (a) and ^{234}Th$_{ex}$ inventory in the sediment (b) of the northern South China Sea during the summer of 2012.

because ^{234}Th activities in freshwater are negligible (Rutgers van der Loeff et al., 2006). Since the currents run predominantly along the shelf (Fig. 1), the transport via water exchange can be further divided into two components: the horizontal shelf-slope water exchange (F_{CS}) that is deemed to be dominated by eddy diffusion, and the advection-dominated along-shelf transport parallel to the coast (F_{AS}). It should be noted that F_{CS} and $F_{Lateral}$ are different as they denote transport fluxes associated with different carriers, i.e., water fluid *versus* particles drifting within the BNL (Walsh et al., 1988). Under steady-state, a mass balance of ^{234}Th over the shelf (Fig. 6) can be set up:

$$F_{Production} + F_{CS} + F_{AS} = F_{Decay} + F_{Sed} + F_{Lateral} \qquad (4)$$

These terms are summarized in Table 2. Their calculation is detailed in three sub-sections: 1) production ($F_{Production}$) and decay (F_{Decay}) in the water column, as well as sedimentary accumulation (F_{Sed}) (Section 4.1.1). These terms are calculated based on the inventories of ^{234}Th and ^{238}U in the shelf water, and the ^{234}Th$_{ex}$ inventories in the sediments; 2) diffusion-dominated horizontal shelf-slope water exchange (F_{CS}) and advective along-shelf transport of water (F_{AS}), which are determined by the direction of net water exchange and the difference of ^{234}Th activities (Section 4.1.2); 3) the unknown flux via cross-shelf particle drifting

($F_{Lateral}$; Section 4.1.3), which is computed as the difference between the other terms (Fig. 6; Table 2). Then, the cross-shelf export fluxes of other particulate components (e.g., POC) can be determined by multiplying $F_{Lateral}$ with the ratio of the component concentration to ^{234}Th activity (unit: μmol dpm^{-1}) in the particles within the BNL of the shelf-slope boundary:

$$F^i_{Lateral} = F_{Lateral} \cdot \frac{C^i_P}{^{234}Th_P} \qquad (5)$$

Here $F^i_{Lateral}$ is the cross-shelf export flux of component i, C^i_P and ^{234}Th$_P$ represent the content of particulate component i and activity of ^{234}Th in the suspended particles respectively within the BNL of the shelf-slope boundary.

4.1.1. Production, decay, and sediment accumulation of ^{234}Th

The estimates of the production, decay, and accumulation of ^{234}Th require the total inventories of ^{238}U and ^{234}Th$_T$ in the water column, as well as the total ^{234}Th$_{ex}$ inventory in the underlying sediments. The calculation of these inventories involving a multiple triangle boxes approach (Tan et al., 2018) was detailed in the Supplementary Material. The reported uncertainties were the standard deviation of the site-
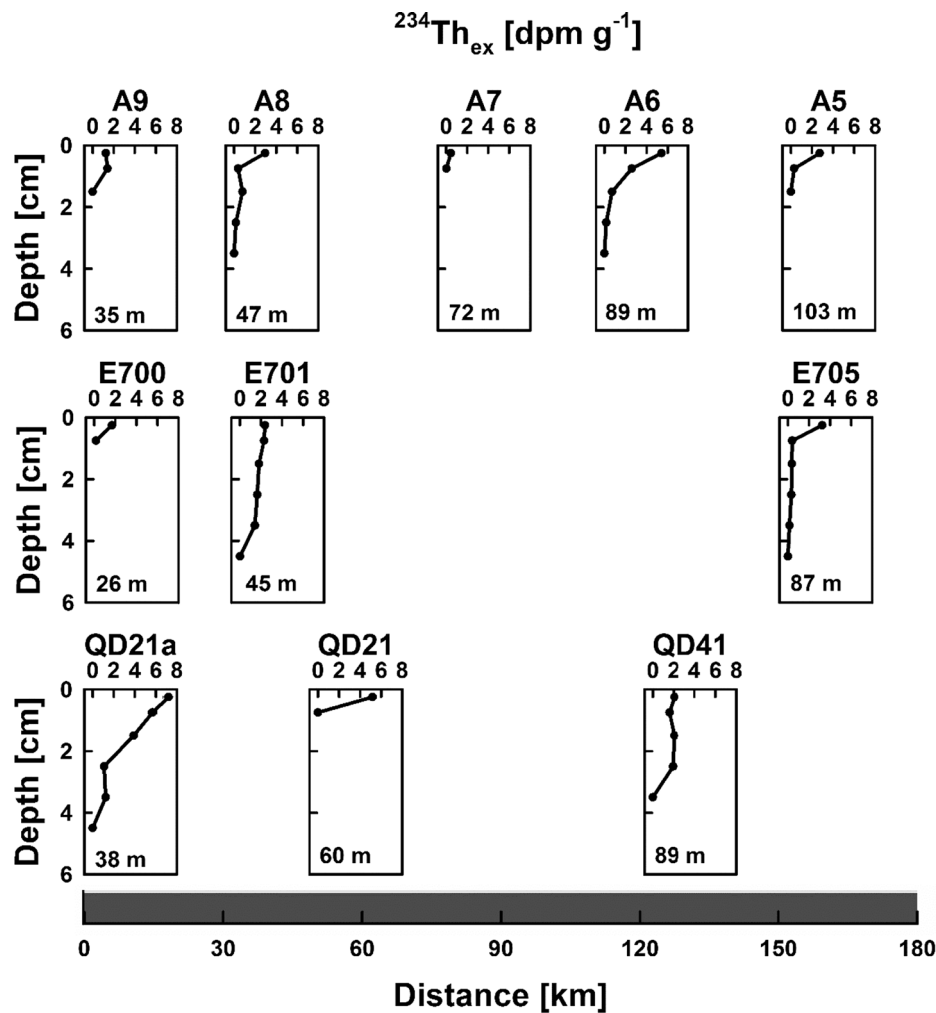
Fig. 5. Depth profiles of $^{234}Th_{ex}$ in the bottom sediments of the northern South China Sea during the summer of 2012. The stations were arranged according to the distance offshore, and the bottom depths were labeled. Note that error bars are shown if larger than the symbol size, but they are negligible on this scale.

specific inventories in the triangle boxes (1 SD, n = 20), which accounts for the uncertainties associated with the spatial coverage of sampling.

The total inventories of ^{238}U and $^{234}Th_T$ in the water column were estimated to be $12.3 \pm 0.3 \times 10^{15}$ and $7.2 \pm 0.2 \times 10^{15}$ dpm, respectively. The area-weighted average production rate ($F_{Production}$) and radioactive decay rate (F_{Decay}), which can be calculated based on the total inventories of ^{238}U and ^{234}Th respectively, the total area, and the decay constant of ^{234}Th ($F_i = \lambda_{Th} \cdot \frac{INV_{Tot}}{S_{Tot}}$), were estimated to be 5820 ± 120 dpm m^{-2} d^{-1} and 3430 ± 100 dpm m^{-2} d^{-1}, respectively (Table 2).

The sediment accumulation rate (F_{Sed}; Fig. 6) was estimated in the same manner of $F_{Production}$ and F_{Decay}. Considering that sandy sediments have a lower binding capacity of thorium isotopes than finer-grain sediments (Cai et al., 2014; Emerson and Young, 1995), two extreme scenarios of $^{234}Th_{ex}$ inventories were evaluated for the stations with sandy sediments and then combined with the locations containing $^{234}Th_{ex}$ measurements to derive the total inventories and subsequently the sediment accumulation rate. In an extreme scenario that the sandy sediments have $^{234}Th_{ex}$ inventories equivalent to the muddy sediments, i.e., I $_{234}Th_{ex}$=3.6 $\pm$ 3.1 $\times$ 10^4 dpm m^{-2}, we derive a total $^{234}Th_{ex}$ inventory of $2.4 \pm 0.1 \times 10^{15}$ dpm or an area-weighted average accumulation rate of 1140 ± 50 dpm m^{-2} d^{-1} (Table 2). In another extreme scenario, the sandy sediments are completely devoid of $^{234}Th_{ex}$, i.e., I $_{234}Th_{ex}$=0, the total inventory and the area-weighted average accumulation rate of ^{234}Th were $1.6 \pm 0.1 \times 10^{15}$ dpm and 770 ± 30 dpm m^{-2} d^{-1}, respectively. The actual values likely lie somewhere in between.

The sedimentary accumulation was a major process responsible for the ^{234}Th removal, accounting for <18% of the total ^{234}Th supply to the shelf water or 25–40% of the removal besides decay. According to the mass balance of ^{234}Th (Eq. (5); Table 2), the two extreme scenarios respectively constrain the lower and upper bounds of the cross-shelf transport flux (see Section 4.1.3).

4.1.2. Horizontal shelf-slope exchange and along-shelf transport of ^{234}Th

The diffusion-dominated horizontal shelf-slope water exchange (F_{CS}) and the advection-dominated along-shelf transport (F_{AS}) are bidirectional (Fig. 1). Whether they act as a source/sink of ^{234}Th for the shelf water depends on the net water transport and the difference of ^{234}Th activities. Transport of waters with higher ^{234}Th activities into the shelf would increase ^{234}Th activities. As such, they would be a source, i.e., F_{CS} and F_{AS} would be positive. Conversely, they would become a sink if the shelf water is replaced by waters with lower activities.

The diffusion-dominated horizontal shelf-slope water exchange (F_{CS}; Fig. 6) can be estimated by multiplying the cross-shelf eddy diffusivity (k_{CS}) by the gradient of ^{234}Th activity ($\frac{\partial A_{234Th_T}}{\partial x}$): $F_{CS} = k_{CS} \times \frac{\partial A_{234Th_T}}{\partial x}$ (see Supplementary Section 1.4 for the calculation of k_{CS} and $\frac{\partial A_{234Th_T}}{\partial x}$). The gradients of ^{234}Th for section A, E7, and QD were estimated to be 0.0062 ± 0.0011 dpm m^{-4} (R^2 = 0.82, n = 9, P < 0.001), 0.0064 ± 0.0013 dpm m^{-4} (R^2 = 0.86, n = 6, P < 0.01), and 0.0061 ± 0.0011 dpm m^{-4} (R^2 = 0.89, n = 6, P < 0.005), respectively. As such, F_{CS} was estimated to be 140 ± 30–280 ± 50 dpm m^{-2} d^{-1} (1 SD; Table 2), which accounted for
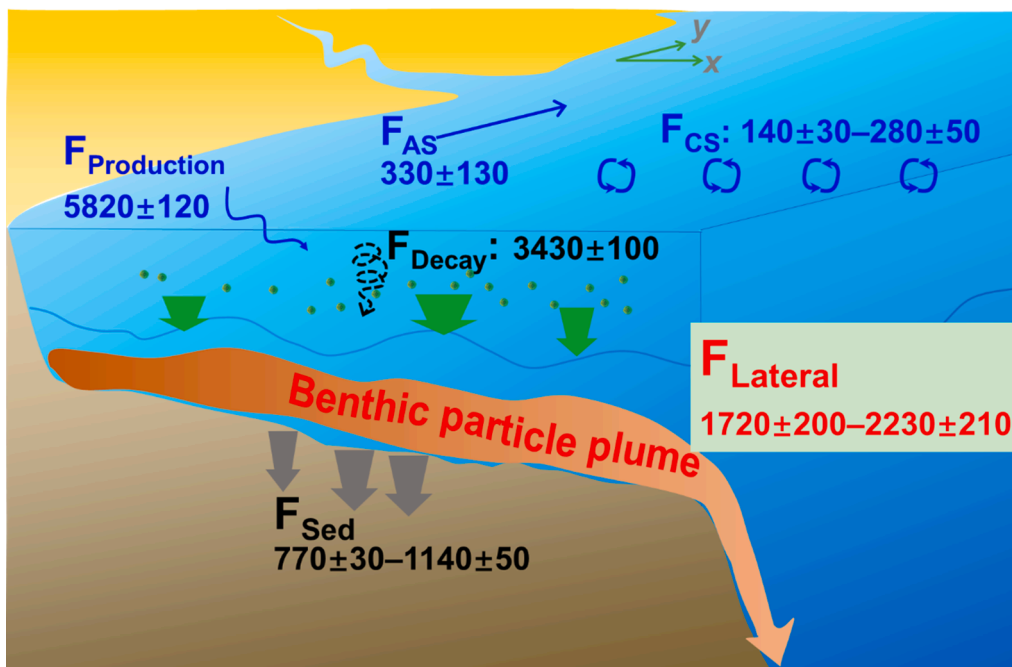
Fig. 6. Schematic of the ^{234}Th mass balance over the northern South China Sea shelf. The numbers denote the ^{234}Th fluxes (unit: dpm m^{-2} d^{-1}). The blue terms represent the supply, while the black and the red terms represent the loss of ^{234}Th.

2.2–4.4% of the total ^{234}Th supply rate.

The along-shelf transport of ^{234}Th (F_{AS}; Fig. 6) depends on the current velocity (v_{AS}) and the activity difference (($\Delta Th_T)_{AS}$) between the two boundaries of the along-shelf current (the inflow through section QD and the outflow through section A). Within the 100 m isobath domain, the currents form a closed cyclonic circulation (Fig. 1), and the difference of ^{234}Th between the inflow and outflow was minimal (Fig. S.5h). As such, the net along-shelf transport of ^{234}Th in this domain could be assumed to be zero. For the stations located within the 100–200 m isobaths, the water column was divided into two layers according to the different velocities of the along-shelf currents and the little change of ^{234}Th activities (Fig. S.5): the upper 10 m with a current velocity of ~ 0.20 m s^{-1}, and the underlying layer from 10 to 75 m with a current velocity of 0.10 m s^{-1} (Ding et al., 2017; Gan et al., 2009). The differences of ^{234}Th activities for these two layers were estimated to be 450 ± 90 and 490 ± 60 dpm m^{-3} using the depth-averaged activities ($\overline{Th_T}$; Supplementary Section 1.4). As such, a maximum of the along-shelf transport of ^{234}Th was estimated to be 20 ± 8 × 10^{12} dpm d^{-1} (1 SD) using the expression: $\sum [v_{AS}\cdot(\Delta Th_T)_{AS}\cdot W\cdot D]$. Here, W denotes the average width of the 100–200 m domain: 57 × 10^3 m; D is the depth of the layers, i.e., 10 and 65 m, respectively. On average, the along-shelf transport resulted in an input of 330 ± 130 dpm m^{-2} d^{-1} (Table 2), which accounted for 5.2% of the total ^{234}Th supply.

4.1.3. Cross-shelf export of particle-associated ^{234}Th from the NSCS shelf

The imbalance between the supply and loss terms detailed above could be reasonably ascribed to the cross-shelf export associated with drifting particles within the BNL ($F_{Lateral}$; Fig. 6). The cross-shelf export flux was estimated to be 110 ± 13–140 ± 13 × 10^{12} dpm d^{-1} with an average of 1720 ± 200–2230 ± 210 dpm m^{-2} d^{-1}, which accounted for ~28–35% of the total ^{234}Th supply (Table 2). It was consistent with the studies in the Bering Sea and the Middle Atlantic Bight, which showed that ~20–30% of the total ^{234}Th or ^{210}Pb supply to the shelf waters were laterally exported to the adjacent slope/basin on seasonal to decadal time scales (Bacon et al., 1994; Baumann et al., 2013). In particular, the cross-shelf export of ^{234}Th exceeded the accumulation into the underlying sediments in the NSCS (Table 2).

Production and decay of ^{234}Th in the water column were the largest terms in the ^{234}Th mass balance. Their uncertainties were well evaluated and not subjected to the sampling resolution since the vertical profiles of ^{234}Th have captured the main distribution features on the shelf. The largest source of the uncertainty associated with $F_{Lateral}$ lies in the sediment accumulation rate (Table 2), which is controlled by the spatial coverage in the sediment sampling. However, the narrow range of $F_{Lateral}$ indicates that our mass balance model is rather insensitive to the sampling resolution. As such, our finding supports the early hypothesis that cross-shelf particle export is a major process responsible for ^{234}Th (and by inference, particulate components, such as POC and trace metals) export out of shelf waters in marginal seas (Walsh et al., 1988; Wong et al., 2000).

4.2. Export flux of particulate organic carbon

4.2.1. Vertical export of ^{234}Th from the euphotic zone

The total supply via horizontal shelf-slope water exchange and net along-shelf transport was included to represent the $V_{^{234}Th}$ term and simply assumed to be evenly distributed in each site's entire water column. This assumption is reasonable as the impact of $V_{^{234}Th}$ should be more significant at shallower depths (e.g., Savoye et al., 2006; and references therein). In this regard, this simplification provides a first-order approximation of this term: $V_{^{234}Th} = \frac{280+330}{H}$.

The vertical fluxes of ^{234}Th from the euphotic zone were estimated to vary from 130 ± 120 to 2300 ± 130 dpm m^{-2} d^{-1} in the NSCS (Table 1), with mean fluxes of 1340 ± 540 dpm m^{-2} d^{-1} (1 SD, n = 18) and 960 ± 1000 dpm m^{-2} d^{-1} (1 SD, n = 3) for the shelf and the slope, respectively. They were consistent with the range obtained in the NSCS during summer (Cai et al., 2015b; Chen et al., 2008). It should be noted that the actual vertical fluxes of ^{234}Th and POC would be underestimated by ~10–33% if the total supply of ^{234}Th via horizontal shelf-slope water exchange and net along-shelf transport was neglected (1010 ± 500 dpm m^{-2} d^{-1} and 870 ± 950 dpm m^{-2} d^{-1} for the shelf and the slope, respectively).

4.2.2. Vertical export of POC from the euphotic zone

POC/^{234}Th$_P$ ratios in suspended particles ranged from 2.0 ± 0.1 to

Table 2
Parameters in the ^{234}Th budget on the shelf of the northern South China Sea during the summer of 2012. See the text for details.

Term	Description	Calculation and value
λ_{Th}	Decay constant of ^{234}Th	0.02876 d^{-1}
S_{Tot}	The total area of the shelf	Sum of the areas in the triangle boxes: $60.7 \pm 1.0 \times 10^9$ m^2
V_{Tot}	The total water volume of the shelf	Sum of the water volumes in the triangle boxes: $5.10 \pm 0.01 \times 10^{12}$ m^3
INV_{Tot}	The total inventory of ^{234}Th or ^{238}U	Sum of the products of the average inventories and the area at each triangle: $INV_{Tot} = \sum \left(\bar{I}_i \times S_i \right)$
L	Length of the shelf-slope boundary at 200 m isobaths	~300 km
τ	Water flushing time of the NSCS shelf	1–2 yr (Cai et al., 2004; Liu et al., 2010)
k_{CS}	Cross-shelf eddy diffusivity	Dividing the total water volume by the water flushing time and the length of the shelf-slope boundary: $k_{CS} = \frac{V_{Tot}}{L \cdot \tau}$. $k_{CS} = 2.3\text{–}4.7 \times 10^4$ m^2 d^{-1}
$\frac{\partial A_{234Th_T}}{\partial x}$	The cross-shelf gradient of ^{234}Th activities	Linear regression of the site-specific depth-averaged activities of water column *versus* distance offshore: $0.0061 \pm 0.0011\text{–}0.0064 \pm 0.0013$ dpm m^{-4}
v_{AS}	Along-shelf current velocity	0.2 m s^{-1} in the upper 10 m, and 0.1 m s^{-1} below 10 m (Ding et al., 2017; Gan et al., 2009)
$(\Delta Th_T)_{AS}$	^{234}Th activity difference between the inflow (Section QD) and the outflow (Section A) of the along-shelf currents	The difference of the depth-averaged activities between section QD and section A for the stations located within the 100–200 m isobaths: 450 ± 90 dpm m^{-3} for the upper 10 m; 490 ± 60 dpm m^{-3} from 10 to 75 m
$F_{Production}$	Supply of ^{234}Th via *in situ* decay of ^{238}U	Multiplying λ_{Th} by the average inventory of ^{238}U: $F_{Production} = \lambda_{Th} \cdot \frac{INV_{Tot, U}}{S_{Tot}}$. It was calculated to be 5820 ± 120 dpm m^{-2} d^{-1}.
F_{CS}	Supply of ^{234}Th via horizontal shelf-slope water exchange	Multiplying the cross-shelf eddy diffusivity by the cross-shelf gradient of ^{234}Th activities: $F_{CS} = k_{CS} \cdot \frac{\partial A_{234Th_T}}{\partial x}$. It was estimated to be $140 \pm 30\text{–}280 \pm 50$ dpm m^{-2} d^{-1}.
F_{AS}	Supply of ^{234}Th via along-shelf current transport	Multiplying the current velocity (v_{AS}) by the activity difference ($(\Delta Th_T)_{AS}$) between the inflow and outflow. The change of ^{234}Th activity limited in the upper 75 m water, as well as the varying current velocities in the upper 10 m layer and the underlying layer from 10 to 75 m were considered. It was estimated to be 330 ± 130 dpm m^{-2} d^{-1}.
F_{Decay}	Loss of ^{234}Th via *in situ* decay	Multiplying λ_{Th} by the area-weighted average inventory of ^{234}Th: $F_{Decay} = \lambda_{Th} \cdot \frac{INV_{Tot, Th_T}}{S_{Tot}}$. The flux was estimated to be 3430 ± 100 dpm m^{-2} d^{-1}.
F_{Sed} *	Loss of ^{234}Th via accumulation into sediments	Multiplying λ_{Th} by the area-weighted average inventory of ^{234}Th$_{ex}$: $F_{Sed} = \lambda_{Th} \cdot \frac{INV_{Tot, 234Th_{ex}}}{S_{Tot}}$. The flux was $770 \pm 30\text{–}1140 \pm 50$ dpm m^{-2} d^{-1}.
$F_{Lateral}$*	Loss via **cross-shelf export** associated with drifting particles	Difference between the known supply and loss terms. That is $F_{Lateral} = F_{Production} + F_{CS} + F_{AS} - F_{Decay} - F_{Sed}$. It was estimated to be $1720 \pm 200\text{–}2230 \pm 210$ dpm m^{-2} d^{-1}.

*: The two extreme scenarios of sandy sediments, i.e., devoid of ^{234}Th$_{ex}$ ($I_{234Th_{ex}}$=0) and that with ^{234}Th$_{ex}$ inventory equal to those in muddy sediments ($I_{234Th_{ex}}$=3.6 ± 3.1 × 10^4 dpm m^{-2}) will set the lower and upper bounds for

^{234}Th accumulation rates into the sediment, and consequently constrain the upper and lower limits of the cross-shelf flux of ^{234}Th.

100 ± 20 µmol dpm^{-1} and decreased with distance offshore (note that the samples with swimmers were excluded in the discussion). They showed remarkably high values in the surface layer of the innermost stations (Fig. S.2b), which was presumably due to the input of terrestrial organic matter and/or phytoplankton growth (Cai et al., 2015; Chen et al., 2008). The ratios at the export horizons varied in the range of 3.7 ± 0.2–43.9 ± 5.1 µmol dpm^{-1} for the shelf, and 5.4 ± 0.4–8.9 ± 0.6 µmol dpm^{-1} for the slope (Table 1). They were comparable to previous high-resolution seasonal measurements conducted in the study area, i.e., 2.6 ± 0.1–41.1 ± 6.5 µmol dpm^{-1} during the summer (Cai et al., 2015b; Chen et al., 2008). According to Eq. (3), the vertical POC fluxes from the euphotic zone were estimated to vary between 1.0 ± 0.9 and 50.7 ± 6.9 mmol m^{-2} d^{-1} (Table 1), and were within the range reported in the SCS and other marginal seas (e.g., Cai et al., 2015b; Le Moigne et al., 2013a; Zhou et al., 2013). On average, the vertical POC fluxes changed from 24 ± 15 mmol m^{-2} d^{-1} (1 SD, n = 18) in the shelf to 7.7 ± 9.4 mmol m^{-2} d^{-1} (1 SD, n = 3) over the slope, following a shift from diatom (size: 2–20 µm) to haptophytes_8 and prasinophytes (<2 µm) in the phytoplankton community structure of the NSCS as reported by Cai et al. (2015b). These fluxes were within the range of 15 ± 16 and 3.6 ± 1.1 mmol m^{-2} d^{-1} for the shelf and basin of NSCS, respectively (Cai et al., 2015b; Zhou et al., 2013).

An 80-day average of NPP from 96 days before sampling was estimated to vary from 20 to 186 mmol C m^{-2} d^{-1} (Table 1; see Supplementary Section 1.1 for the calculations). High NPP occurred in the innermost stations, where primary production was presumably stimulated by the terrestrial input of nutrients (Cai et al., 2015; Chen et al., 2008). The total POC flux and the total NPP were estimated to be 1580 ± 57 × 10^6 and 3040 ± 110 × 10^6 mol C d^{-1} (1 SD, n = 20), respectively. They were equivalent to an area-weighted average of 26 ± 1 mmol C m^{-2} d^{-1} for vertical POC flux and 50 ± 2 mmol C m^{-2} d^{-1} for NPP, which are in line with previous measurements in the study area during summer (Cai et al., 2015b). On average, the efficiency of vertical POC export from the euphotic zone was 52%, which was higher than those in the SCS basin (8–31%; Li et al., 2018; Liu et al., 2002) and comparable to the efficiencies in other shelves (e.g., ~40% in the shelf off Peru; Black et al., 2018).

4.2.3. Cross-shelf export of POC

We assume that cross-shelf transport processes mainly occur via drifting particles within the BNL (Section 4.1), which are more vulnerable to cross-shelf transport than sinking particles. The low POC/^{234}Th$_P$ ratios within the BNL of the shelf-slope boundary (Fig. S.2b), which could be the result of preferential remineralization of POC relative to Th (e.g., Buesseler et al., 2006; Cai et al., 2006a) and/or binding of ^{234}Th to lithogenic material (Passow et al., 2006), are considered to be representative for particles laterally exported out of the shelf. As such, the POC/^{234}Th ratios used here will provide a first-order approximation of the final cross-shelf POC flux. The ratios within the BNL of the shelf-slope boundary (i.e., from 100 m to the bottom of A4, E707, and QD71) varied between 2.0 ± 0.1 and 8.8 ± 0.5 µmol dpm^{-1}, and averaged 5.0 ± 2.3 µmol dpm^{-1} (1 SD, n = 12). Using this range and the total cross-shelf flux of ^{234}Th (Table 2) yields a cross-shelf POC flux of 210 ± 30–1200 ± 130 × 10^6 mol d^{-1} (average ± 1 SD: 600 ± 210 × 10^6 mol d^{-1}), which was 7–39% of the total NPP in the shelf water. It corresponded to an area-weighted average cross-shelf flux of 3.5 ± 0.4–20 ± 2 (average ± 1 SD: 9.9 ± 3.4) mmol m^{-2} d^{-1}, which is roughly 0.8–4.7 times the reported vertical POC fluxes in the basin (e.g., Cai et al., 2015b). This result is in line with an estimate that in the intermediate and deep waters of the NSCS, the laterally transported POC was ~1–4 times higher than the POC settled from the euphotic zone (Shen et al., 2020; and references therein).

This cross-shelf transport occurred below 200–1000 m and within

500 m above the seafloor as indicated by the turbidity at the slope stations (Fig. S.6), which is consistent with previous studies showing similar depths of lateral transport in the SCS (Ma et al., 2017; Shih et al., 2019; and references therein). Therefore, POC laterally exported out of the shelf could be trapped within the intermediate and deep waters (>500 m) for several decades considering the long residence times of these water parcels (~40 years; Liu and Gan, 2017). It could also serve as a major energy and organic carbon source that enhances the dark carbon fixation in the deep SCS for millennia (Jiao et al., 2010; Shen et al., 2020). In this regard, cross-shelf transport could play an essential role in the long-term carbon sequestration in the SCS.

The cross-shelf POC flux was comparable to the ^{234}Th-derived vertical fluxes without the influence of episodic events (e.g., bloom) in the global ocean (Fig. S.7), i.e., 5.4 ± 8.9 (n = 202), 5.3 ± 6.1 (n = 270), 6.6 ± 8.7 (n = 172), and 7.0 ± 6.5 (n = 56) mmol m^{-2} d^{-1} during the spring, summer, autumn, and winter, respectively (updated from Le Moigne et al., 2013a). However, it was lower than the vertical fluxes in some marginal seas influenced by upwelling (e.g., >30 mmol m^{-2} d^{-1} in the Peruvian shelf; Black et al., 2018), and/or by phytoplankton bloom (e.g., up to 41 mmol m^{-2} d^{-1} in the North Atlantic; Buesseler et al., 1992). Note that the choice of the reference depth matters for the ^{234}Th-derived vertical fluxes and the BCP efficiencies (Buesseler et al., 2020). Though the dataset of the global ocean assessed at fixed depths of 100/150 m or the base of the euphotic zone differs between sites, the straightforward comparison here illustrates the key role of cross-shelf export in the ocean BCP.

The cross-shelf POC flux in the NSCS was comparable to those from the eastern Bering Sea shelf, the Chukchi Sea, and the shelf of Middle Atlantic Bight during spring and summer, as well as that from the Hebrides Shelf west of Scotland during autumn (Table 3). However, there is no work performed in winter or regarding the seasonal variation in a single region. A compilation of other studies and our result showed a relatively narrow range of cross-shelf POC flux (10 ± 5 mmol m^{-2} d^{-1}; 1 SD, n = 6), though they were occupied from subtropical to arctic marginal seas in different seasons. It was approximately three times the annual fluxes from the global shelves estimated based on a mass balance of carbon (Chen et al., 2003; Table 3). In this regard, our results argue for caution in global extrapolations from limited regional data and urge high data coverage over global shelves to provide accurate quantification of the cross-shelf POC flux on a global scale (Liu et al., 2010; and references therein).

5. Concluding remarks

Cross-shelf transport of POC is essential in controlling the export efficiency of primary production on shelves. Nonetheless, the flux and its contribution to the biological pump remains poorly constrained. Here, the radionuclide ^{234}Th was used to quantify the cross-shelf flux of POC from the northern South China Sea (NSCS), where this process is ubiquitous but not quantified. On a seasonal basis, cross-shelf transport is a major process responsible for the removal of ^{234}Th (and by inference, particulate components like POC) from the shelf water. Horizontal shelf-slope exchange and along-shelf transport of water were taken into consideration in the estimate of vertical fluxes of ^{234}Th and POC, otherwise fluxes would have been underestimated by ~10–33%. The vertical POC flux via vertical export from the euphotic zone was estimated to be 26 ± 1 mmol m^{-2} d^{-1}, while that via cross-shelf transport along the BNL was 3.5 ± 0.5–20 ± 2 mmol m^{-2} d^{-1}. The cross-shelf exported POC was presumably transported into the intermediate/deep waters that have long residence times. Thus, it plays an essential role in long-term carbon storage in the NSCS. The compilation of the measurements regarding cross-shelf POC transport suggested that this cross-shelf flux might be larger than the previous global estimate (Chen et al., 2003). However, we call for caution against extrapolating limited regional data to a global scale and urge improved data coverage for an accurate evaluation of the role of the cross-shelf POC transport in the

Table 3
Comparison of the cross-shelf POC fluxes over the global shelves.

Study area	Flux [mmol m^{-2} d^{-1}]	Method	Time	Reference
eastern Bering Sea shelf	18 ± 41	^{234}Th mass balance	Spring and summer	(Baumann et al., 2013)
Chukchi Sea	12 ± 16	^{234}Th and carbon mass balance	Spring and summer	(Lepore et al., 2007)
Mid-Atlantic Bight shelf	6.4 ± 7.8	^{210}Pb mass balance	Spring and summer	(Bacon et al., 1994)
Hebrides shelf, west of Scotland	2.1–22.3 (10.0 ± 7.4)	Ekman drainage	Autumn	(Painter et al., 2016)
East China Sea	2.1 ± 1.1	Carbon mass balance	Annual	(Chen et al., 2003)
Global shelves	3.0 ± 1.5	Carbon mass balance	Annual	(Chen et al., 2003)
northern South China Sea shelf	3.5 ± 0.5–20 ± 2 (9.9 ± 3.4)	^{234}Th mass balance	Summer	This study

Fluxes in the brackets denote the average values.

global ocean.

Author contributions

P. Cai and Q. Hong jointly conceived this study. Q. Hong, S. Peng, and D. Zhao performed sampling and analysis. Q. Hong wrote the manuscript with inputs from P. Cai.

Declaration of Competing Interest

The author declare that there is no conflict of interest.

Acknowledgment

References

Aller, R.C., Cochran, J.K., 2019. The critical role of bioturbation for particle dynamics, priming potential, and organic C remineralization in marine sediments: local and basin scales. Front. Earth Sci. SC-SWITZ, 7.
Bacon, M.P., Belastock, R.A., Bothner, M.H., 1994. ^{210}Pb balance and implications for particle transport on the continental shelf, U.S. Middle Atlantic Bight. Deep Sea Res. II 41, 511–535.
Baumann, M.S., Moran, S.B., Kelly, R.P., Lomas, M.W., Shull, D.H., 2013. ^{234}Th balance and implications for seasonal particle retention in the eastern Bering Sea. Deep Sea Res. II 94, 7–21.
Behrenfeld, M.J., Falkowski, P.G., 1997. Photosynthetic rates derived from satellite-based chlorophyll concentration. Limnol. Oceanogr. 42, 1–20.
Black, E.E., Buesseler, K.O., Pike, S.M., Lam, P.J., 2018. ^{234}Th as a tracer of particulate export and remineralization in the southeastern tropical Pacific. Mar. Chem. 201, 35–50.
Buesseler, K.O., Antia, A.N., Chen, M., Fowler, S.W., Gardner, W.D., Gustafsson, O., Harada, K., Michaels, A.F., der Loeff, M.R., Sarin, M., 2007. An assessment of the use of sediment traps for estimating upper ocean particle fluxes. J. Mar. Res. 65, 345–416.
Buesseler, K.O., Bacon, M.P., Kirk Cochran, J., Livingston, H.D., 1992. Carbon and nitrogen export during the JGOFS North Atlantic Bloom experiment estimated from ^{234}Th:^{238}U disequilibria. Deep-Sea Res. 39, 1115–1137.
Buesseler, K.O., Benitez-Nelson, C.R., Moran, S.B., Burd, A., Charette, M., Cochran, J.K., Coppola, L., Fisher, N.S., Fowler, S.W., Gardner, W.D., Guo, L.D., Gustafsson, Ö.,

Lamborg, C., Masque, P., Miquel, J.C., Passow, U., Santschi, P.H., Savoye, N., Stewart, G., Trull, T., 2006. An assessment of particulate organic carbon to thorium-234 ratios in the ocean and their impact on the application of ^{234}Th as a POC flux proxy. Mar. Chem. 100, 213–233.

Buesseler, K.O., Boyd, P.W., Black, E.E., Siegel, D.A., 2020. Metrics that matter for assessing the ocean biological carbon pump. Proc. Natl. Acad. Sci. USA, 201918114.

Burdige, D.J., 2006. Geochemistry of marine sediments. Princeton University Press, Princeton.

Cai, P., Dai, M., Chen, W., Tang, T., Zhou, K., 2006a. On the importance of the decay of ^{234}Th in determining size-fractionated C/^{234}Th ratio on marine particles. Geophys. Res. Lett. 33, L23602.

Cai, P., Dai, M., Lv, D., Chen, W., 2006b. An improvement in the small-volume technique for determining thorium-234 in seawater. Mar. Chem. 100, 282–288.

Cai, P., Rutgers van der Loeff, M., Stimac, I., Nöthig, E.M., Lepore, K., Moran, S.B., 2010. Low export flux of particulate organic carbon in the central Arctic Ocean as revealed by ^{234}Th:^{238}U disequilibrium. J. Geophys. Res. 115, C10037.

Cai, P., Shi, X., Hong, Q., Li, Q., Liu, L., Guo, X., Dai, M., 2015a. Using ^{224}Ra/^{228}Th disequilibrium to quantify benthic fluxes of dissolved inorganic carbon and nutrients into the Pearl River Estuary. Geochim. Cosmochim. Acta 170, 188–203.

Cai, P., Shi, X., Moore, W.S., Peng, S., Wang, G., Dai, M., 2014. ^{224}Ra:^{228}Th disequilibrium in coastal sediments: implications for solute transfer across the sediment–water interface. Geochim. Cosmochim. Acta 125, 68–84.

Cai, P., Zhao, D., Wang, L., Huang, B., Dai, M., 2015b. Role of particle stock and phytoplankton community structure in regulating particulate organic carbon export in a large marginal sea. J. Geophys. Res. 120, 2063–2095.

Cai, W.-J., 2011. Estuarine and coastal ocean carbon paradox: CO$_2$ sinks or sites of terrestrial carbon incineration? Annu. Rev. Mar. Sci. 3, 123–145.

Cai, W.-J., Dai, M., Wang, Y., Zhai, W., Huang, T., Chen, S., Zhang, F., Chen, Z., Wang, Z., 2004. The biogeochemistry of inorganic carbon and nutrients in the Pearl River estuary and the adjacent Northern South China Sea. Cont. Shelf Res. 24, 1301–1319.

Chen, C.-T.A., Liu, K.-K., Macdonald, R., 2003. Continental Margin Exchanges. In M.J.R. Fasham (Ed.), Ocean Biogeochemistry: The Role of the Ocean Carbon Cycle in Global Change (pp. 53-97). Berlin, Heidelberg: Springer Berlin Heidelberg.

Chen, J.H., Lawrence Edwards, R., Wasserburg, G.J., 1986. ^{238}U, ^{234}U and ^{232}Th in seawater. Earth Planet. Sci. Lett. 80, 241–251.

Chen, W., Cai, P., Dai, M., Wei, J., 2008. ^{234}Th/^{238}U Disequilibrium and Particulate Organic Carbon Export in the Northern South China Sea. J. Oceanogr. 64, 417–428.

Chen, Y.-L., 2005. Spatial and seasonal variations of nitrate-based new production and primary production in the South China Sea. Deep Sea Res. I 52, 319–340.

DeMaster, D.J., McKee, B.A., Nittrouer, C.A., Qian, J., Cheng, G., 1985. Rates of sediment accumulation and particle reworking based on radiochemical measurements from continental shelf deposits in the East China Sea. Cont. Shelf Res. 4, 143–158.

Ding, Y., Bao, X., Yao, Z., Zhang, C., Wan, K., Bao, M., Li, R., Shi, M., 2017. A modeling study of the characteristics and mechanism of the westward coastal current during summer in the northwestern South China Sea. Ocean Sci. J. 52, 11–30.

Emerson, H.S., Young, A.K., 1995. Method development for the extraction of naturally occurring radionuclides in marine sediments. Sci. Total Environ. 173–174, 313–322.

Falkowski, P.G., Flagg, C.N., Rowe, G.T., Smith, S.L., Whitledge, T.E., Wirick, C.D., 1988. The fate of a spring phytoplankton bloom: export or oxidation? Cont. Shelf Res. 8, 457–484.

Gan, J., Li, L., Wang, D., Guo, X., 2009. Interaction of a river plume with coastal upwelling in the northeastern South China Sea. Cont. Shelf Res. 29, 728–740.

Hong, Q., Cai, P., Shi, X., Li, Q., Wang, G., 2017. Solute transport into the Jiulong River estuary via pore water exchange and submarine groundwater discharge: New insights from ^{224}Ra/^{228}Th disequilibrium. Geochim. Cosmochim. Acta 198, 338–359.

Honjo, S., Eglinton, T.I., Taylor, C.D., Ulmer, K.M., Sievert, S.M., Bracher, A., German, C. R., Edgcomb, V., Francois, R., Iglesias-Rodriguez, M.D., Van Mooy, B., Repeta, D.J., 2014. Understanding the role of the biological pump in the global carbon cycle: an imperative for ocean science. Oceanogr. 27, 10–16.

Huang, D., Du, J., Deng, B., Zhang, J., 2013. Distribution patterns of particle-reactive radionuclides in sediments off eastern Hainan Island, China: implications for source and transport pathways. Cont. Shelf Res. 57, 10–17.

Hung, C.C., Gong, G.C., 2010. POC/^{234}Th ratios in particles collected in sediment traps in the northern South China Sea. Estuar. Coast. Shelf Sci. 88, 303–310.

Jahnke, R.A., 2010. Global Synthesis. In: Liu, K.-.-K., Atkinson, L., Quiñones, R., Talaue-McManus, L. (Eds.), Carbon and Nutrient Fluxes in Continental Margins. Springer, Berlin Heidelberg, pp. 597–615.

Jiao, N., Herndl, G.J., Hansell, D.A., Benner, R., Kattner, G., Wilhelm, S.W., Kirchman, D. L., Weinbauer, M.G., Luo, T., Chen, F., Azam, F., 2010. Microbial production of recalcitrant dissolved organic matter: long-term carbon storage in the global ocean. Nat. Rev. Microbiol. 8, 593–599.

Knap, A., Michaels, A., Close, A., Ducklow, H., Dickson, A., 1996. Protocols for the joint global ocean flux study (JGOFS) core measurements. JGOFS Report No. 19 (Reprint of the IOC Manuals and Guides No. 29, UNESCO 1994).

Le Moigne, F.A.C., Henson, S.A., Sanders, R.J., Madsen, E., 2013a. Global database of surface ocean particulate organic carbon export fluxes diagnosed from the ^{234}Th technique. Earth Syst. Sci. Data 5, 295–304.

Le Moigne, F.A.C., Villa-Alfageme, M., Sanders, R.J., Marsay, C., Henson, S., García-Tenorio, R., 2013b. Export of organic carbon and biominerals derived from ^{234}Th and ^{210}Po at the Porcupine Abyssal Plain. Deep Sea Res. I 72, 88–101.

Lepore, K., Moran, S.B., Grebmeier, J.M., Cooper, L.W., Lalande, C., Maslowski, W., Hill, V., Bates, N.R., Hansell, D.A., Mathis, J.T., Kelly, R.P., 2007. Seasonal and

interannual changes in particulate organic carbon export and deposition in the Chukchi Sea. J. Geophys. Res. 112.

Li, T., Bai, Y., He, X., Chen, X., Chen, C.-T., Tao, B., Pan, D., Zhang, X., 2018. The Relationship between POC Export Efficiency and Primary Production: Opposite on the Shelf and Basin of the Northern South China Sea. Sustainability 10, 3634.

Liu, K.K., Atkinson, L., Quiñones, R.A., Talaue-McManus, L., 2010. Carbon and nutrient fluxes in continental margins: a global synthesis. Springer, Berlin Heidelberg.

Liu, K.K., Chao, S.Y., Shaw, P.T., Gong, G.C., Chen, C.C., Tang, T.Y., 2002. Monsoon-forced chlorophyll distribution and primary production in the South China Sea: observations and a numerical study. Deep Sea Res. I 49, 1387–1412.

Liu, Z., Gan, J., 2017. Three-dimensional pathways of water masses in the South China Sea: a modeling study. J. Geophys. Res. 122, 6039–6054.

Ma, H., Yang, W., Zhang, L., Zhang, R., Chen, M., Qiu, Y., Zheng, M., 2017. Utilizing ^{210}Po deficit to constrain particle dynamics in mesopelagic water, western South China Sea. Geochem. Geophys. Geosyst. 18, 1594–1607.

Maiti, K., Buesseler, K.O., Pike, S.M., Benitez-Nelson, C., Cai, P., Chen, W., Cochran, K., Dai, M., Dehairs, F., Gasser, B., 2012. Intercalibration studies of short-lived thorium-234 in the water column and marine particles. Limnol. Oceanogr. Methods 10, 631–644.

Owens, S.A., Pike, S., Buesseler, K.O., 2015. Thorium-234 as a tracer of particle dynamics and upper ocean export in the Atlantic Ocean. Deep Sea Res. II 116, 42–59.

Painter, S.C., Hartman, S.E., Kivimäe, C., Salt, L.A., Clargo, N.M., Bozec, Y., Daniels, C.J., Jones, S.G., Hemsley, V.S., Munns, L.R., Allen, S.R., 2016. Carbon exchange between a shelf sea and the ocean: the Hebrides Shelf, west of Scotland. J. Geophys. Res. 121, 4522–4544.

Passow, U., Dunne, J., Murray, J.W., Balistrieri, L., Alldredge, A.L., 2006. Organic carbon to ^{234}Th ratios of marine organic matter. Mar. Chem. 100, 323–336.

Pates, J.M., Muir, G.K.P., 2007. U-salinity relationships in the Mediterranean: implications for ^{234}Th:^{238}U particle flux studies. Mar. Chem. 106, 530–545.

Pike, S.M., Buesseler, K.O., Andrews, J., Savoye, N., 2005. Quantification of ^{234}Th recovery in small volume sea water samples by inductively coupled plasma-mass spectrometry. J. Radioanal. Nucl. Ch. 263, 355–360.

Puigcorbé, V., Benitez-Nelson, C.R., Masqué, P., Verdeny, E., White, A.E., Popp, B.N., Prahl, F.G., Lam, P.J., 2015. Small phytoplankton drive high summertime carbon and nutrient export in the Gulf of California and Eastern Tropical North Pacific. Global Biogeochem. Cycles 29, 1309–1332.

Rutgers van der Loeff, M.M., Sarin, M.M., Baskaran, M., Benitez-Nelson, C., Buesseler, K. O., Charette, M., Dai, M., Gustafsson, Ö., Masque, P., Morris, P.J., Orlandini, K., Rodriguez y Baena, A., Savoye, N., Schmidt, S., Turnewitsch, R., Vöge, I., Waples, J. T., 2006. A review of present techniques and methodological advances in analyzing ^{234}Th in aquatic systems. Mar. Chem. 100, 190–212.

Savoye, N., Benitez-Nelson, C., Burd, A.B., Cochran, J.K., Charette, M., Buesseler, K.O., Jackson, G.A., Roy-Barman, M., Schmidt, S., Elskens, M., 2006. ^{234}Th sorption and export models in the water column: a review. Mar. Chem. 100, 234–249.

Schlitzer, R., 2018. Ocean Data View. http://odv.awi.de.

Schmidt, S., Chou, L., Hall, I.R., 2002. Particle residence times in surface waters over the north-western Iberian Margin: comparison of pre-upwelling and winter periods. J. Marine. Syst. 32, 3–11.

Shen, J., Jiao, N., Dai, M., Wang, H., Qiu, G., Chen, J., Li, H., Kao, S.-J., Yang, J.-Y.T., Cai, P., Zhou, K., Yang, W., Zhu, Y., Liu, Z., Chen, M., Zuo, Z., Gaye, B., Wiesner, M. G., Zhang, Y., 2020. Laterally transported particles from margins serve as a major carbon and energy source for dark ocean ecosystems. Geophys. Res. Lett. 47 e2020GL088971.

Shih, Y.-Y., Lin, H.-H., Li, D., Hsieh, H.-H., Hung, C.-C., Chen, C.-T.A., 2019. Elevated carbon flux in deep waters of the South China Sea. Sci. Rep. 9, 1–8.

Tan, E., Wang, G., Moore, W.S., Li, Q., Dai, M., 2018. Shelf-Scale Submarine Groundwater Discharge in the Northern South China Sea and East China Sea and its geochemical impacts. J. Geophys. Res. 123, 2997–3013.

Walsh, J.J., Biscaye, P.E., Csanady, G.T., 1988. The 1983–1984 shelf edge exchange processes (SEEP)—I experiment: hypotheses and highlights. Cont. Shelf Res. 8, 435–456.

Wang, J., Du, J., Baskaran, M., Zhang, J., 2016. Mobile mud dynamics in the East China Sea elucidated using ^{210}Pb, ^{137}Cs, ^{7}Be, and ^{234}Th as tracers. J. Geophys. Res. 121, 224–239.

Waples, J.T., Benitez-Nelson, C., Savoye, N., Rutgers van der Loeff, M.M., Baskaran, M., Gustafsson, Ö., 2006. An introduction to the application and future use of ^{234}Th in aquatic systems. Mar. Chem. 100, 166–189.

Wei, C.L., Lin, S.Y., Sheu, D.D., Chou, W.C., Yi, M.C., Santschi, P.H., Wen, L.S., 2011. Particle-reactive radionuclides (^{234}Th, ^{210}Pb, ^{210}Po) as tracers for the estimation of export production in the South China Sea. Biogeosciences 8, 3793–3808.

Wong, G.T.F., Chao, S.-Y., Li, Y.-H., Shiah, F.-K., 2000. The Kuroshio edge exchange processes (KEEP) study — an introduction to hypotheses and highlights. Cont. Shelf Res. 20, 335–347.

Zhong, Y., Chen, Z., Li, L., Liu, J., Li, G., Zheng, X., Wang, S., Mo, A., 2017. Bottom water hydrodynamic provinces and transport patterns of the northern South China Sea: evidence from grain size of the terrigenous sediments. Cont. Shelf Res. 140, 11–26.

Zhou, K., Dai, M., Kao, S.-J., Wang, L., Xiu, P., Chai, F., Tian, J., Liu, Y., 2013. Apparent enhancement of ^{234}Th-based particle export associated with anticyclonic eddies. Earth Planet. Sci. Lett. 381, 198–209.

Zhou, K., Dai, M., Maiti, K., Chen, W., Chen, J., Hong, Q., Ma, Y., Xiu, P., Wang, L., Xie, Y., 2020. Impact of physical and biogeochemical forcing on particle export in the South China Sea. Prog. Oceanogr. 187, 102403.